

# Development Stage and Application of a Virtual Process Chain for RTM Components

L. Kärger, D. Magagnato, S. Galkin

(Karlsruhe Institute of Technology (KIT), Institute of Vehicle System Technology, Karlsruhe Germany);

F. Fritz

(Institute of Textile Technology and Process Engineering (ITV), Denkendorf, Germany)

A. Schön

(University of Stuttgart, Institute of Aircraft Design (IFB), Stuttgart, Germany)

A. Oeckerath, K. Wolf

(Fraunhofer Institute for Algorithms and Scientific Computing (SCAI), St. Augustin, Germany)

F. Henning

(Fraunhofer Institute for Chemical Technology (ICT), Pfingstfeld, Germany)

## Summary:

The development of high-performance composite components made by Resin Transfer Molding (RTM) is very time consuming and cost intensive. This high development effort is caused by numerous manual iteration steps which are still necessary to find the optimal design in conjunction with the optimal process control. Additionally, composite components are highly oversized due to the discrepancy between the real material behavior, which is largely influenced by the processing history, and the idealized models used in structural simulation. During the draping process, the fiber alignment is considerably modified, resulting in varying fiber orientations, varying fiber volume contents and local draping effects like gaps, overlaps and fiber waviness. These changes in material characteristics influence the mechanical performance and need to be considered for sizing and virtual validation of RTM structures.

In this work a continuous virtual CAE process chain is presented. The current development focusses on a holistic integration and validation of the essential simulation steps to suitably predict and consider all relevant manufacturing effects. The fiber alignment is determined by draping simulation and transferred to molding simulation and structural simulation of the RTM component. Geometry data as well as material data are transferred between the finite element models by using a uniform exchange data format and a mapping algorithm. The importance of considering manufacturing effects is demonstrated by applying the continuous CAE chain to a complexly curved RTM part. Structural simulation results of both, CAE chain models with mapped fiber orientations and conventional FE models with simply projected fiber orientations, are validated by comparison with experimental results.

## Keywords:

CAE chain, RTM, process simulation, draping, molding, structural simulation, FE mapping

## 1 Introduction

Carbon-fiber reinforced plastics (CFRP) provide a considerable potential for mass-reduction of high performance structures. Their excellent mass-specific properties can be tailored to the actual needs and make them well qualified for use in lightweight constructions. However, the economical exploitation of these theoretical potentials is currently limited by insufficiencies of manufacturing processes, by lack of knowledge of the material behavior and by insufficient prediction of the structural performance. These weaknesses can only be solved by further improving the understanding in the fields of methods, materials and processes and by establishing a close collaboration in between these three disciplines [1]. In this respect, the development of a virtual process chain (CAE chain) needs to be built on an interdisciplinary knowledge base, not only in the field of process and structural simulation, but also in production technology and material understanding.

To make high-performance composite materials economic for large-scale production, it is essential to reduce the overall development costs. A continuous CAE chain offers a high potential to accelerate the large number of development loops via simulation of the real processes. For metal processing several holistic simulation platforms with FE-based data exchange have already been established (e.g. FEDES [2], MpCCI [3], ICME [4]). Also in the field of injection molding, there are software packages available, which enable the transformation of process simulation results to the FE models of structural simulation (e.g. DIGIMAT, SIGMA SOFT). While CAE chains for metal processing and injection molding are already established and applicable for commercial process development, the development of CAE chains for high-performance FRPs is just at the beginning. First work on that field has been performed at the TU Munich in cooperation with BMW [5], [6], at DLR Braunschweig [7] and by the present authors within the Technology Cluster Composites TC<sup>2</sup> in Baden-Württemberg [8]. While the transfer of fiber orientations already works quite reliably, further local fiber effects (like fiber volume content, ply thickness, fiber waviness, overlaps and gaps) have not yet been considered. There is furthermore a shortage of continuous experimental validation throughout the process chain from draping up to structural performance.

This work presents a continuous virtual process chain developed by the Technology Cluster Composites TC<sup>2</sup>, a consortium of research institutes in Baden Württemberg. The CAE chain had previously been introduced at the NAFEMS World Congress 2013 [8]. Since then, a comprehensive experimental test program has been conducted by manufacturing and loading a convex-concave component. This complex 3D-curved structure has been used to validate the CAE chain throughout the manufacturing process, from draping, over molding up to the final structural behavior. Just curing and distortion is not yet included, but subject of ongoing investigations.

## 2 Development of the CAE chain

### 2.1 Overview

The overall scheme of the CAE chain established by the Technology Cluster Composites TC<sup>2</sup> is shown in Fig. 1. One long-term goal of the CAE chain is to use the connections between the simulation domains for iterative optimization over multiple steps. However, the present focus of research is the reliable prediction of process results and the reliable flow of information from left to right. The development chain starts with the design phase, where an initial geometry and layup is given to the first simulation domain, the draping simulation. If the draping process is feasible for the given design, the fiber orientations, fiber volume contents etc. serve as input for the molding simulation. After molding simulation, the computed information goes further to curing simulation. The curing simulation models chemical and thermal shrinkage after demolding, resulting in residual stresses and distortions. The acquired information is transferred to the structural simulation, where the final structural performance is assessed. If the required structural performance can be validated, everything is ready for manufacturing. Otherwise, if enhancements are necessary, the design will be accordingly adapted. In the present work, an application of the CAE chain to a complex 3D structure is presented: Draping, molding and structural simulation are performed, where draping simulation results are mapped to the subsequent simulation steps and the simulation results of the mapped models are compared to simulation results of reference models as well as to experimental results of structural tests.

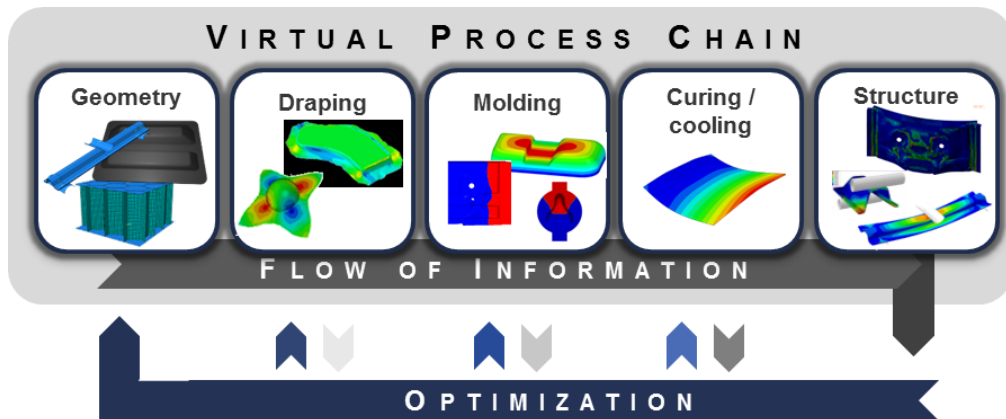


Fig. 1: Virtual Process Chain combining design, process and structural simulation. Current state: flow of information from left to right. Long-term target: Optimization loops over multiple simulation steps during the design phase to reduce overall development cost.

The simulation steps are connected with each other by the transfer of relevant simulation results. In addition to an elementary data transformation, the simulation results have to be converted due to differing types of FE meshes. Therefore, two intermediate steps are necessary, cf. [8]. First, a uniform exchange format needs to be established to transfer the data. Second, a uniform mapping software needs to be used to suitably convert the data from one FE mesh to another. As interchange format the vtk ASCII format has been selected. In order to conduct the mapping, the mapping library MpCCI MapLib is used [9]. The transformation process between two adjacent simulation domains is illustrated in Fig. 2.

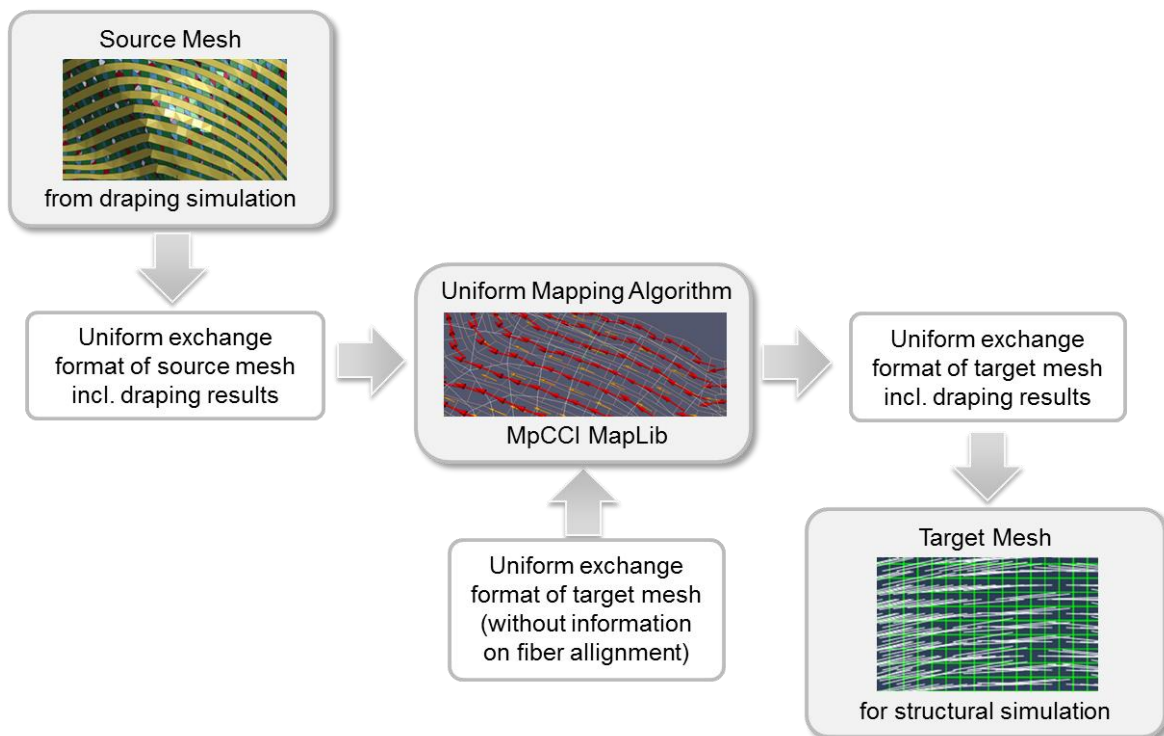


Fig. 2: Data conversion process to transfer information from one simulation domain (e.g. draping simulation, left) to another simulation domain (e.g. structural simulation, right) by using a uniform mapping software (MpCCI MapLib, middle) in combination with a uniform exchange format.

## 2.2 Interchange format

To make the data transformation process independent of the applied FE software, a neutral file format is chosen. The requirements for such a unified file format are based on the needs for data mapping, particularly on the used data types of the FE software and on the mapping software. Hence, all possible element types from various FE programs need to be reflected. Additionally, all relevant composite parameters have to be considered, like fiber orientations as vectors or fiber volume fraction and thicknesses as scalars. As a suitable format, the vtk file-format from the Visualization Toolkit project has been selected. All elements and value types are supported and the mapping library MpCCI MapLib has a native reader/writer for this format. Additionally, with ParaView a powerful open source scientific visualization program is available in order to visualize, compare and assess the data of the neutral vtk format.

To generate and to translate the vtk files, software-specific transformation scripts have been developed, each dedicated to the applied software package (e.g. LS-DYNA, PamForm, PamRTM, OpenFoam, Abaqus and others) used for a certain simulation domain. While the transformation of the mesh and the composite information into the vtk format is relatively simple, the transformation of the mapping results from vtk format into the respective input deck of the FE software is much more complex. For example, the handling of gaps and overlaps has to be performed in this step. The transformation script is responsible to solve these issues adequately and to generate a correct FE input deck which is processable by the FE software. More information on the used features from vtk file-format and on the transformation scripts can be found in [8].

## 2.3 Mapping

The **MpCCI MapLib** [9] is a generic numerical C++ library, which allows to utilize the mapping technology coming from Fraunhofer SCAI's multi-physics code coupling solutions in own CAE mapping applications. The library supports all standard mesh and element types and provides various forms of neighborhood calculation between differently discretized models. It is organized in different classes following an object-oriented approach. It also provides a wide range of input and output interfaces to native FE solvers as well as neutral file formats like vtk.

To perform a data mapping at first a donor (source) and an acceptor (target) geometry needs to be defined as MapLib mesh. Having both meshes defined, a neighborhood has to be computed. The kind of neighborhood does typically depend on the mapping scheme that is used for data transfer. Table 1 gives an overview about mapping schemes currently implemented in MapLib with its characteristics. If the location of the input quantity, i.e. source quantity, does not match required algorithm location, data is automatically converted using the Finite Element shape function approach.

Mapping Scheme	Source Location	Target Location	Interpolation Order	Advantages	Disadvantages
Shape Function	Node	Node	Element order	Conserves precision of solution	Not conservative
Weighted k-Nearest	Node	Node	1	Robustness	Lower order
Weighted Element	Element	Element	1	Robustness	Lower order
Element Center	Node	Element	Element order	Conserves precision of solution	Not conservative
Flux	Node	Node	0	Conservative	Discontinuous

Table 1: Basic mapping schemes in MapLib

A mapping process for a layered structure of composites has to satisfy additional modelling characteristics during the simulation process chain. Typically in draping simulation each textile layer is modelled individually as part of a stack with different shapes. Through in-plane displacement between different layers, the total number of layers across the component, especially in the edge areas, may be non-uniform. In contrast, a model for structural simulation, representing the same layered structure, can be realized using a single shell element.

So, for an accurate transfer of element- and layer-specific data the mapping need to be performed layer-wise where also absent layers are taken into account. In [8] was shown, that the *weighted k-nearest* mapping scheme of MapLib produced best results when transferring fiber orientation information between differently discretized models. Fig. 3 illustrates the mapping result for a reference fiber orientation when mapping from a fine source onto a coarser target model.

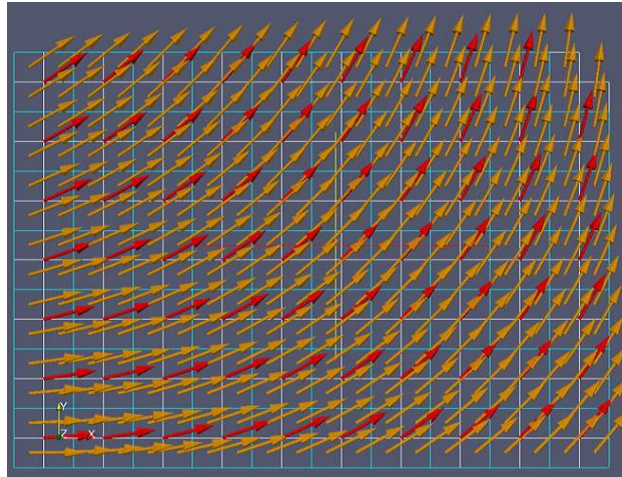


Fig. 3: Mapping from a fine source mesh (white mesh, orange fiber orientation vectors) to a coarse target mesh (light-blue mesh, red fiber orientation vectors) adopted from [8].

### 3 Draping Simulation

#### 3.1 Draping Simulation Method

To suitably predict the molding and the structural behavior of a composite component, it is necessary the detailed fiber architecture of the textile needs to be known. Therefore, a forming simulation is required at the starting point of the simulation chain. Different approaches for the draping simulation are known. One widely used approach is the time-efficient kinematic draping also known as geometric draping. However, the results of the kinematic draping simulation are calculated only regarding the final geometry, without considering material properties of the fabric as well as process specific boundary conditions. The kinematic approach delivers short calculation time but unsatisfying results for complex geometries. To incorporate the material properties and the boundary conditions, a finite element model has been developed to improve the prediction of the fiber re-orientation. Finite element simulation offers the possibility to recreate the complex material properties of the dry textile regarding different stiffness values for tension, shear and bending.

For primarily unidirectional non crimp fabrics fiber slipping is the dominating effect during the draping process. Best results are obtained using a very detailed model of the textile construction. In this mesoscopic approach the stitching and the yarn are modelled separately and are coupled by contact (Fig. 4 left, [10], [8]). This approach offers the possibility to define different properties along the material directions and incorporate the slipping of the fibers on shear loading. However, this model is of no practical use since its calculation time is out of range on large parts.

Therefore, a macroscopic replacement has been designed preserving most of the original behavior (Fig. 4, right). The model consists of shell stripes modelling the unidirectional bundles of carbon fibers and connecting them with beams representing the gap between the bundles caused by the stitching. The material direction is defined by the edge of the shell element along the shell strip.

Usually the beam and shell models implemented in finite element codes are based on the theory of small deformations based on the major assumption that “plane sections remain plane”. A textile bent along the fiber axis behaves more like bending of a pile of paper where plane sections do not remain plane. Thus textiles do not comply with the assumption made. To achieve an acceptable bending behavior, the modelling of tension and bending need to be decoupled. Therefore the shell stripes representing the fiber bundles as well as the beams in the gap are carried out “double layered” to account for this separation. In reality the width of the gap is very small in relation to the width of the fiber bundle. For example, the pitch of the fiber bundles may be 5.1 mm where the width of the fiber bundles varies around 5 mm leaving a gap of about 0.1 mm.

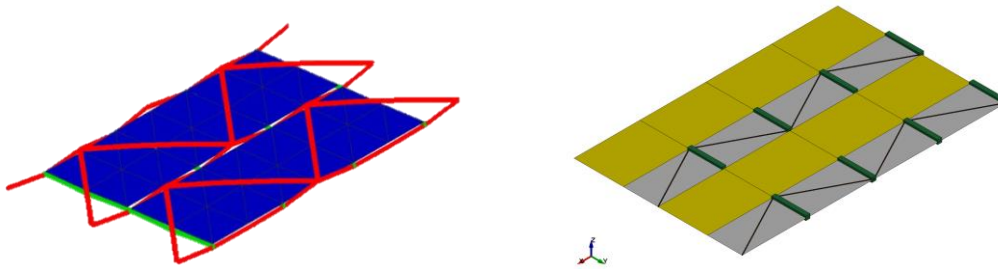


Fig. 4: Modelling of unidirectional non crimp fabric using different approaches (left: meso model [10] applied in [8], right: macro model as applied in this work)

In explicit FE codes the stability and the overall calculation time depends on the size of the time steps. In LS-DYNA the critical time step size is a function of the element size. Smaller elements lead to prolonged calculation times. Hence, in this model the representation of the gap is modelled oversized. Additionally, to obtain a continuous shell surface a null-shell is added to the gap allowing a relatively fast and stable contact treatment among the individual plies and with the tooling.

The material parameters needed for this work have been determined by simulation of tension tests as well as the ASTM D1388 cantilever bending test, all carried out at the fiber angles of  $0^\circ$ ,  $45^\circ$  and  $90^\circ$ .

### 3.2 Draping Application and Results

To analyze the effects of deep-drawing textile structures, a 3D-curved convex-concave component has been developed and analyzed, see Fig. 5. The convex-concave geometry contains the difficulties encountered in complexly shaped automotive parts including features such as embossments and ribbing. For manufacturing, first a preforming process was performed, followed by a resin transfer molding (RTM) process. One cavity filling of the RTM mold contains two stacked preforms each consisting of four plies only distinguishable by the reversed ply order. Two stacking sequences have been investigated, one unidirectional (UD)  $[0^\circ]$  8 ply layup and one quasi-isotropic (QI)  $[0^\circ/90^\circ/45^\circ/-45^\circ]_s$  layup.

The experimental draping process has been performed at IFB Stuttgart, being one partner of the TC<sup>2</sup> consortium serving as the basis of the virtual process. In the initial state of the stamping process, the pile of NCF textiles is clamped between the blank holder and the die. The die is held down by multiple pneumatic and electrically driven linear actuators. The punch rises from underneath and depresses the textile. In the region of the ribbing, a movable die is positioned on the textile which is fixed in the initial state slightly above the textile and starts moving, after the ribbing has been formed. The movement is synchronized with the punch to keep the textile clamped between the punch and the movable die. A tensional load is applied to several fiber bundles to prevent wrinkling. Therefore clamps with weights, connected via a steel wire, have been attached at eight different locations.

The draping simulation of the stamping process is conducted with the modelling approach described in section 3.1. It shows analogous folds, gaps and compression zones like the experiments conducted in a parallel project of TC<sup>2</sup> (Fig. 5 left). Fig. 5.b shows a comparison between the simulation result (red) and a CT scan of the outer layer of the manufactured part (green). While the overall fiber orientation is globally well predicted, there are still local differences between simulation and experiment, particularly at critical regions like in Fig. 5.b, where distinct surfaces from all three spatial directions come together. One main reason for these still existing discrepancies is the merging and compression process between draping and molding, which is not yet virtually described but which results in an alteration of the fiber architecture. Furthermore, local draping effects like fiber waviness cannot be predicted by current draping simulation methods.

In order to transfer the draping simulation results to the subsequent simulation steps, the fiber orientations are defined by the first two nodal coordinates of the shell strips which represent the fiber bundles. This information is extracted as a vector in global coordinates and exported to vtk file.

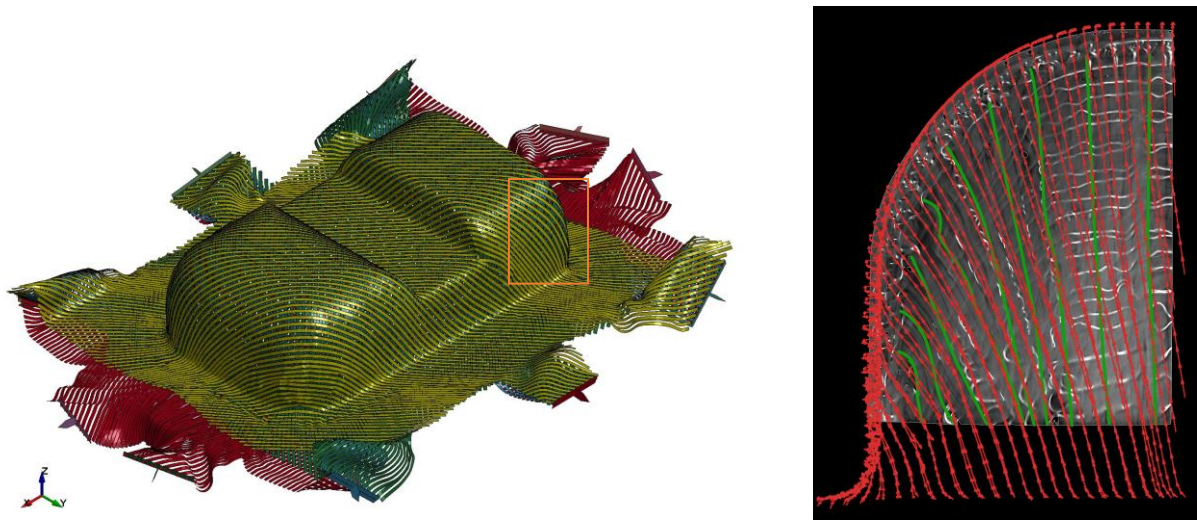


Fig. 5: Draping simulation results (a) Global fiber architecture of plies 1 to 4. (b) Corner detail comparing the simulation result (red) with a CT scan (green) of the inner  $0^\circ$  ply of one manufactured part.

## 4 Molding Simulation

### 4.1 Molding Simulation Method

Subsequent to draping simulation, a molding simulation is necessary to model and to optimize the infiltration of the matrix material (e.g. epoxy resin) through the fiber preform during RTM manufacturing. The infiltration process is usually modeled by the law of Darcy [11]. Relevant material parameters are the viscosity of the resin and the permeability  $K$  of the fibers. The viscosity is set constant as a first step. In reality it will vary due to different temperatures changes and due to the beginning curing reaction. The permeability of the textile is an anisotropic tensor, which is dependent on the fiber volume fraction and on the fiber direction, cf. Fig. 6. For the unidirectional fibers, the direction with best permeability  $K_1$  is parallel to the fibers and the worst permeability  $K_2$  is normal to the fiber direction. The permeability  $K_3$  in thickness direction can be neglected, because of the small thickness of the composites parts [12].

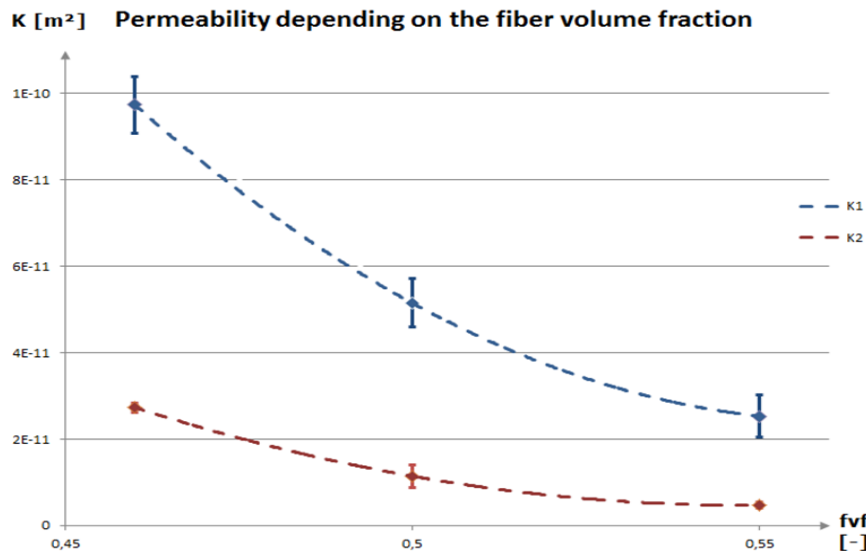


Fig. 6: Measured permeability depending on fiber volume fraction of the used non-crimp fabric [1].

### 4.2 Molding Application and Results

The alignments of the fibers have a big influence on the progress of the resin flow front. To properly consider the actually preformed fiber alignment, the first step is to map the local fiber orientations from the draping mesh to the mesh of the molding simulation, see Fig. 7. This has to be done for each of the eight layers of the preform. After that and the following format conversion, the mesh with the

updated fiber orientations can be imported into PAM-RTM, the software for molding simulation used in this work.

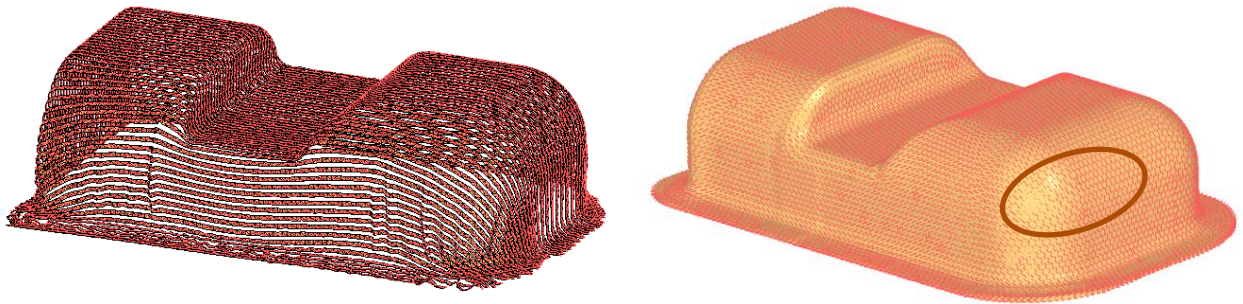


Fig. 7: Transfer of the local fiber orientations. Left: draping mesh, right: molding mesh.

Fig. 8 shows a part of the mesh of the convex-concave component, where on the right the fiber orientations are imported from the draping simulation ("draping model"). To demonstrate the improvements by applying the CAE chain, a reference model is created, where the global fiber orientation of each layer is projected in each element on the surface of the mesh, see Fig. 8 left. This is an easy approach to model the fiber orientation if no draping simulation is available.

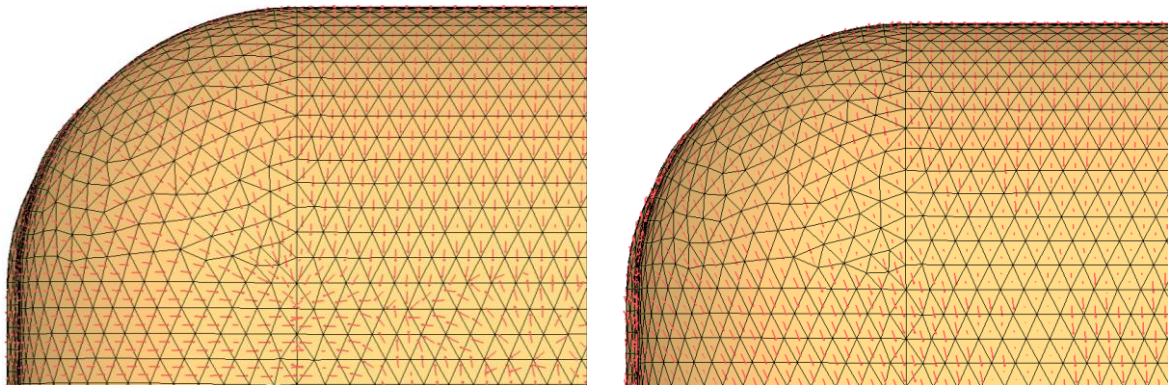


Fig. 8: Local fiber orientation of reference model (left) and draping model (right).

In Fig. 9 the flow front of molding simulation is illustrated for both models at the same time step. The flow front of the reference model is more affected by the curvature of the part (i.e. slow flow progress at high curvatures), while the flow front of the draping model is more homogeneous.

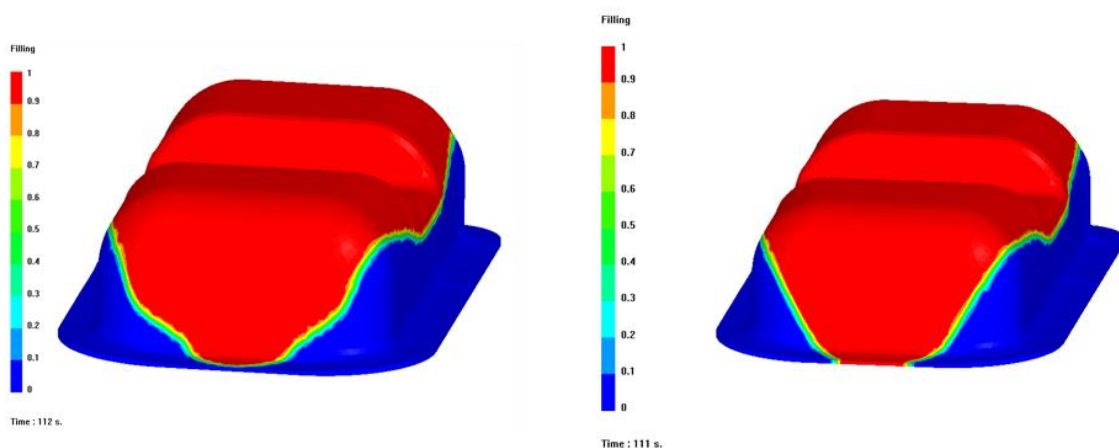


Fig. 9: Molding simulation results of reference model (left) and draping model (right)

The fiber volume fraction is set constant to an average value of 47 % in the first step. In reality it will vary due to different cavity thickness and due to material accumulation in the curved areas of the component, resulting from the draping and compression process. This has an even bigger influence to the molding simulation. The influence of fiber volume fraction, in connection with experimental validation, will be focused in an upcoming publication.

## 5 Structural Simulation

### 5.1 Structural Simulation Method

Structural analysis is performed implicitly by using the software package ABAQUS Standard. Depending on the transverse dimensions and on the rate of transverse stresses, the structural component is meshed by shell elements and/or solid elements. In the case of shell elements, as used in this work, the Hashin failure initiation criterion [13] and a damage evolution model by Lapczyk [14] are applied to analyze failure and damage. This material model was evaluated and parameterized for the applied material in previous work. In [15] it had been shown by the authors that the model is sufficiently accurate to reproduce test results for unidirectional (UD) and quasi-isotropic (QI) laminates under tension and bending, as well as for structural hat profiles under bending. Table 2 to Table 5 show the parameters of the used material (Toray T620 fibers and Sika Biresin CR170 resin / CR150-3 hardener) as applied in the model. Due to a varying thickness over the component, the samples have different fiber volume contents (FVC, 55% and 46%). Therefore, respective homogenized stiffness components and strength components in fiber direction were determined. For failure transverse to the fibers, in-situ strength values according to [16] and [17] have been computed. The interlaminar fracture toughness  $G^c$  in Table 5 was determined by ENF tests [18]. To consider delamination between each layer, a cohesive surface behavior is used.

FVC	$E_1$ [GPa]	$E_2$ [GPa]	$G_{12}$ [GPa]	$G_{13}$ [GPa]	$G_{23}$ [GPa]	$\nu_{12}$ [-]
46%	94.3	7.7	3.3	3.3	2.2	0.31
55%	111.1	8.6	3.9	3.9	2.5	0.29

Table 2: Elastic properties.

FVC	$R_{1+}$ [MPa]	$R_{1-}$ [MPa]	$R_{2+}$ (UD + in-situ) [MPa]	$R_{2-}$ [MPa]	$R_{12}$ (UD + in-situ) [MPa]	$R_{23}$ [MPa]
46%	1418	816	54.5 (UD)	153.5	60 (UD)	22.4
			107.2 (QI middle layers)		93 (QI middle layers)	
			136.1 (QI other layers)		107.4 (QI other layers)	
55%	1670	957.3	54.5 (UD)	153.5	60 (UD)	22.4
			111.1 (QI middle layers)		93.4 (QI middle layers)	
			157.1 (QI other layers)		114.3 (QI other layers)	

Table 3: Unidirectional and in-situ strengths.

$G_{1+}$ [kJ/m <sup>2</sup> ]	$G_{1-}$ [kJ/m <sup>2</sup> ]	$G_{2+}$ [kJ/m <sup>2</sup> ]	$G_{2-}$ [kJ/m <sup>2</sup> ]
240	17	0.7	1.8

Table 4: Intralaminar fracture toughness.

$t_h$ [MPa]	$t_s$ [Mpa]	$t_t$ [Mpa]	$G^c$ [kJ/m <sup>2</sup> ]
54.5	68	22.4	1.5

Table 5: Interlaminar strengths and interlaminar fracture toughness.

### 5.2 Structural Application and Results

To evaluate the effects of differing fiber architectures from draping onto the structural simulation, a number of test coupons were cut out in relevant areas and tested under tension, see Fig. 10. These areas were chosen due to deviations between projected fiber orientations (reference model) and mapped fiber orientations (draping model, see Z2 samples in Fig. 10). For validation of the previously parameterized material model, also coupons in the valley of the convex-concave component, i.e. with almost ideal fiber orientation, where chosen to be tested (Z1 samples).

Static tension tests were conducted at Fraunhofer EMI as one partner of the TC<sup>2</sup> consortium. Samples with both unidirectional (UD) and quasi-isotropic (QI) layouts were investigated.

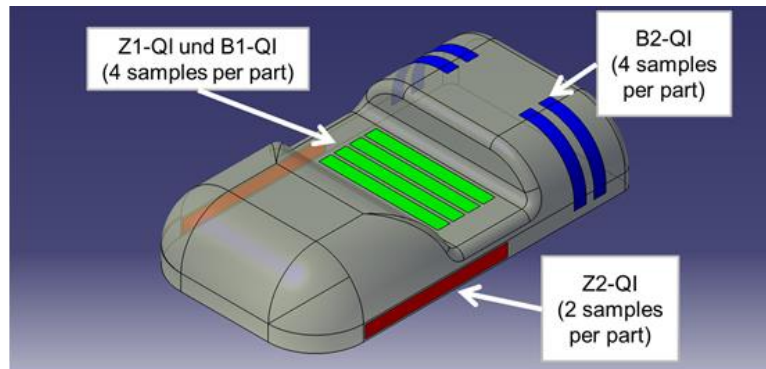


Fig. 10: Coupon samples of the convex-concave component with quasi-isotropic (QI) layout.

The FE models for each coupon sample were separated from the rest of the FE model of the complete convex-concave component. By using the mapping tools, the fiber orientations were transferred to the model's mesh as distribution tables. Each layer has its own fiber orientation, is modelled by separate continuum shell elements and is connected with surface cohesive behavior to the other layers. A static implicit solver was used with a viscous regularization to achieve convergence. To compare the effects of the mapping with the simply projected fiber orientations, both configurations were simulated.

The experimental and simulation results are shown in Fig. 11 and Fig. 12, where all results from one sample configuration are combined in one diagram. The samples of the Z1 area (Fig. 11 left) have almost ideal fiber orientation in 0° direction, resulting in just small differences in stiffness and strength between mapped and projected fibers. By comparing the simulation results of the Z2 samples, the projected fiber orientations (green curves) predict much higher global stiffness and much higher global strength than the mapped fiber orientations (blue curves). In the case of projected fiber orientations, the final failure is always fiber failure. In contrast, for the Z2 coupons with mapped fibers, a matrix failure leads to fatal failure. Simulation of the QI Z2 coupons has additionally shown, that neglecting delamination would lead to a 100 MPa higher maximum strength. Therefore, delamination should be always considered for QI laminates, when the load is not directly introduced into the fibers.

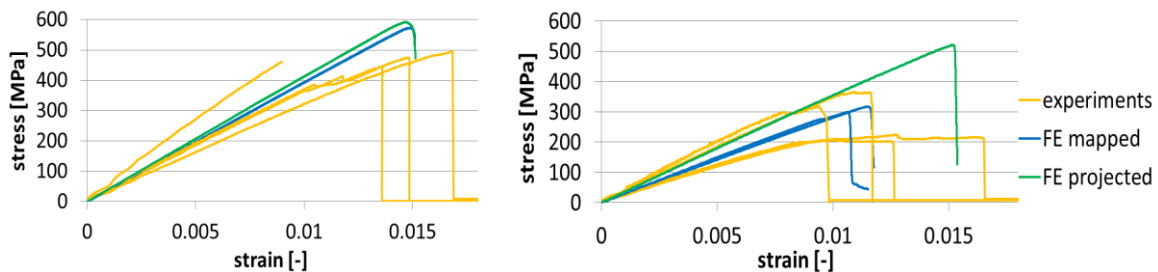


Fig. 11: Quasi-isotropic laminate results (left: Z1 area, right: Z2 area).

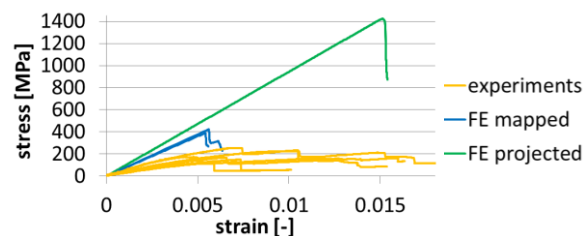


Fig. 12: Unidirectional laminate results (Z2 area).

By comparing experimental results and simulation results with mapped fibers, the predictability of the simulation depends on fiber orientation and laminate layout. The simulation results of the QI laminates in the Z1 area (Fig. 11 left) have a higher stiffness and strength than the experimental results. This can be explained by an actual lower FVC in the coupons than estimated from the thickness of the coupons and/or by a higher fiber misalignment than predicted by the draping simulation. This assumption still has to be validated by FVC measurements. By slightly reducing the FVC, the

simulation would fit to the experiments in both stiffness and strength since the maximum strain of 1.5% is still fiber dominated.

The Z2 samples with QI laminate layup (Fig. 11 right) show a difference between the coupons on each side of the convex-concave component. One side has higher stiffness and strength (two upper experimental curves). The other side has much lower stiffness and strength, but much higher maximum strain (two lower experimental curves). The simulation predicts no such big difference; both sides are almost equal in stiffness, but there is a difference in maximum strength. This leads to the conclusion that draping simulation predicts a globally more symmetric fiber architecture than the real draping process actually provides.

The greatest deviation between simulation and experiments is observed in the case of a UD laminate (Fig. 12). Applying the simply projected fiber orientations leads to very unrealistic results. The simulation with mapped fibers shows a better agreement with experimental results, but there are still higher stiffness and higher strength predicted. The reason for the deviation between mapped simulation results and experiments is just a small difference between the fiber orientations in reality and the fiber orientations of the draping simulation. The difference appears by comparing the fracture angles (see Fig. 13), which is driven by the fiber orientation. While draping simulation predicts an angle of  $\sim 10^\circ$  deviation from the ideal  $0^\circ$  fiber orientation, the experiments show angles between  $15^\circ$  and  $27^\circ$ . If UD fibers are used for reinforcement of structural components then the knowledge of the fiber orientation is the primary factor for a reliable prediction of the maximum strength of the component.

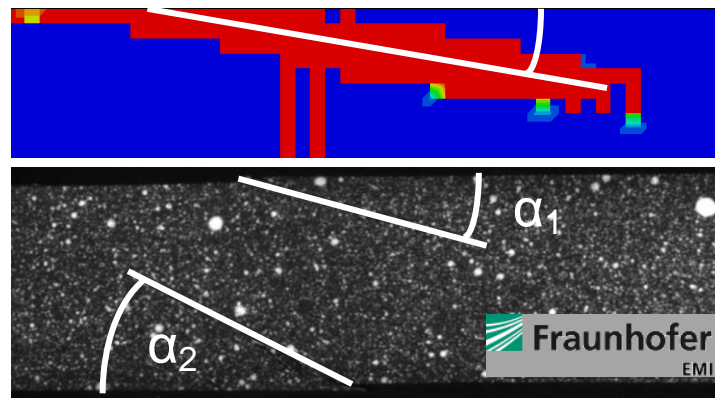


Fig. 13: Fracture angles comparison between simulation and experiment for UD coupons

## 6 Conclusions

A continuous virtual CAE process chain has been developed for high-performance composite components made by Resin Transfer Molding (RTM). The transformation of CAE data between different FE meshes is realized by the mapping library MpCCI MapLib. To make the CAE chain independent of the applied FE software packages, a uniform data structure has been defined in vtk ASCII. In the present work, the CAE chain has been applied to a three-dimensionally curved, convex-concave composite component and has been validated by subsequent tests along the process chain. Fiber orientations were computed by draping simulation, validated by CT scans and, finally, transferred to molding and to structural simulation by applying the CAE chain. For molding and structural performance, the simulation results of the CAE chain models with mapped fiber orientations were compared to simulation results of conventional FE models with simply projected fiber orientations. The resulting molding behavior as well as the resulting mechanical behavior showed a strong dependency on the implemented fiber alignments. For further evaluation, the structural simulation results were compared to experimental results for a number of test coupons. These test coupons were cut out in relevant areas and tested under tension. The experimental results confirmed that the reference models with projected fiber orientations predict much too high global stiffness and much too high global strength in areas where fiber orientations differ from the ideal  $0^\circ$  direction. The simulation results of the models with mapped fibers, on the other hand, were much closer to experimental results. However, a few discrepancies were still detected. They are caused by small differences between the fiber orientations in reality and the fiber orientations of the draping simulation and/or by differing fiber volume contents, other than estimated from the thickness of the coupons. Future research will concentrate on enhancing the draping simulation and validating the fiber volume content. There is also a large number of further manufacturing effects like fiber waviness and gaps, which need to be suitably considered.

## 7 Acknowledgements

The presented work has been performed as part of the R&D activities in in the framework of the “Technology Cluster Composites Baden-Wuerttemberg TC<sup>2</sup>”. The titles of the involved research project is “RTM CAE/CAx – Establishment of a continuous CAE/CAx chain for the RTM technology, against the background of manufacturing high-performance composite materials”. This project is funded by the state government of Baden-Wuerttemberg in Germany and the Baden-Wuerttemberg Stiftung gGmbH. The authors are grateful to the partners of the TC<sup>2</sup> consortium, IFB Stuttgart, HS Esslingen and Fraunhofer ICT, IWM and EMI, who have conducted manufacturing and experimental tests. Furthermore, the help of our student assistants Yasin Gündüz and Lukas Ast in simulation tasks is gratefully acknowledged.

## 8 References

- [1] Henning, F.; Bernath, A.; Chaudhari, R.; Kärger, L.; Magagnato, D.; Schirmaier, F.: “An integrated development approach to combine design, manufacturing and validation of high-pressure RTM composite structures”. Proceedings SAMPE TECH Conference, Seattle, 2014.
- [2] Afazov, S.; Becker, A. and Hyde, T.: “Development of a Finite Element Data Exchange System for chain simulation”. Advances in Engineering Software, 47, pp. 104-113, 2012.
- [3] Fraunhofer SCAI: “MpCCI 4.3.1-2 Documentation, Part I Overview”. Sankt Augustin: Fraunhofer SCAI, 2014.
- [4] Schmitz, G. J.; Prahl, U.: “Integrative Computational Materials Engineering: Concepts and Applications of a Modular Simulation Platform”. Weinheim: Wiley-VCH, 2012.
- [5] Hinterhölzl, R. M.: “Simulation of Draping, Infiltration and Curing of Composites. FACC Technical Colloquium “Advances in Composites”, Salzburg, AT; 2012.
- [6] Dix M, Bickerton S, Tryfonifis M, Hinterhölzl R.: “Consistent Virtual CFRP Process Chain Using a Modular CAE Interface”. Proceedings NAFEMS World Congress, Salzburg, AT; 2013.
- [7] Wille, T.; Kärger, L.; Hein, R.: “Composite Process Chain Towards As-Built Design”, In: Wiedemann, M.; Sinapius, M. (eds.) Adaptive, Tolerant and Efficient Composite Structures. Springer Verlag Berlin Heidelberg, pp. 199-210. ISBN 978-3-642-29189-0, 2013.
- [8] Kärger, L.; Schön, A.; Fritz, F.; Böehler, P.; Maganato, D. Fischer, S.; Henning, F.: “Virtual Process Chain for an integrated assessment of high-performance composite structures”, NAFEMS World Congress, Salzburg, 2013.
- [9] Spiess, H; Oeckerath, A. and Landvogt, B.: “Mapping Library Manual Version 2010.1”, Fraunhofer SCAI, Sankt Augustin, 2012.
- [10] P. Böehler, F. Härtel, P. Middendorf: “Mesoskopisches Drapieren“. SAMPE Symposium Stuttgart, 2014.
- [11] Darcy, H: “Les Fontaines Publique de la Ville de Dijon”, Dalmant Paris, 1856.
- [12] Magagnato, D., Frey, M., Bernath, A., Steibler, P., Henning, F.: “Experimentelle und numerische Untersuchung der Infiltration bei der RTM-Fertigung, 19. Symposiums Verbundwerkstoffe und Werkstoffverbunde“, DGM , Karlsruhe, 2013.
- [13] Hashin, Z.: “Failure Criteria for Unidirectional Fiber Composites”, J. Appl. Mech. 47: 329-334, 1980.
- [14] Lapczyk, I.; Hurtado, J. A.: “Progressive damage modeling in fiber-reinforced materials”, Composites Part A 38(11): 2333–2341, 2007.
- [15] Galkin, S.; Kärger L.; Henning F.; Häfele, P.; Gall, M.; Voß, H.: “Parametrisierung und Evaluierung der in ABAQUS implementierten Schädigungsmodelle für Faserverbundkunststoffe auf Basis umfangreicher Charakterisierungs- und Validierungsversuche“. NAFEMS DACH, Bamberg, 2014.
- [16] Camanho, Pedro P.; Dávila, Carlos G.; Pinho, Silvestre T.; Iannucci, Lorenzo; Robinson, Paul: “Prediction of in situ strengths and matrix cracking in composites under transverse tension and in-plane shear”. Composites Part A: Applied Science and Manufacturing 37 (2): 165–176, 2006.
- [17] Pinho, S.; Darvizeh, R.; Robinson, P.; Schuecker, C.; Camanho, P.: “Material and structural response of polymer-matrix fibre-reinforced composites.” Journal of Composite Materials 46: 2313–2341, 2012.
- [18] Gall, M.; Galkin, S.; Hohe, J.; Kärger, L.: “Fracture mechanics evaluation of RTM-CFRP materials for large-scale production of automotive structures”. 7th International Conference on Fracture of Polymers, Composites and Adhesives, ESIS, Les Diablerets, 2014.